

Watching proteins function with picosecond time-resolved X-ray crystallography

Philip Anfinrud¹, Friedrich Schotte¹, and Michael Wulff²

¹ Laboratory of Chemical Physics, NIDDK, National Institutes of Health, Bethesda, MD 20892, USA

E-mail: anfinrud@nih.gov; schotte@nih.gov

² European Synchrotron Radiation Facility, Grenoble Cedex 38043, FRANCE

E-mail: wulff@esrf.fr

Abstract. We have developed the method of picosecond time-resolved crystallography and used this technique to investigate structural dynamics in biological macromolecules at ambient temperature. Time-resolved snapshots of myoglobin following flash photolysis of the CO adduct were determined with 150 ps time resolution and $< 2 \text{ \AA}$ spatial resolution. The structures reveal numerous sites in which CO becomes transiently trapped, as well as correlated motion of the protein side chains. When a single point mutation was introduced in a position near the binding site (L29F), the departure of CO from the primary docking site was significantly accelerated. The dramatic differences in the correlated protein displacements provide a structural explanation for these kinetic differences.

1. Introduction

Ultrafast phenomena in systems ranging from small molecules in the gas phase to proteins in the condensed phase have been characterized spectroscopically with numerous pump-probe methods. The transitions probed, whether rotational, vibrational, or electronic, can reveal much about the dynamics of the phenomenon being studied, but generally provide rather limited information about structural evolution. For crystalline samples, X-ray diffraction provides an extremely powerful structural tool, with \AA spatial resolution attainable with proteins containing thousands of atoms. We have recently extended the technique of nanosecond X-ray crystallography [1] to the picosecond time domain, and used this method to probe structural changes in myoglobin and its L29F mutant. Myoglobin is a heme protein that reversibly binds small ligands such as O_2 , CO, and NO. The photosensitivity of the ligand bond [2] and the reversibility of ligand binding allow structural changes associated with ligand migration to be determined with picosecond time-resolved crystallography. By comparing the structural evolution of Mb with one of its mutants, we aim to assess the functional role of highly conserved side chains in the vicinity of the active binding site. When Leu (L) in the 29 position is replaced by Phe (F), i.e., L29F MbCO, the oxygen binding affinity is enhanced by a factor of 10 [3] and the ligand escape dynamics are dramatically altered [4]. Here, we report 150-ps time-resolved structures of both wild-type MbCO and L29F MbCO. Their structural differences on the picosecond time scale are far greater than those observed on the ns time scale.

2. Experimental Methods

The experiments reported here were conducted on the time-resolved ID09B beam line at the European Synchrotron and Radiation Facility (ESRF) in Grenoble, France. Diffraction images were acquired using the pump-probe method: a picosecond laser pulse (2-100 ps; ~ 580 nm) triggered ligand dissociation in a ~ 250 micron P6 MbCO crystal and a variably delayed X-ray pulse (150 ps; 0.79 Å with a 3.5% bandwidth) probed its structure (see Figure 1). Synchrotron

Radiation consists of X-ray bursts of ps duration, but at repetition rate far too high for pump-probe experiments. At the ESRF, this rate is 355 kHz or 1.42 MHz, depending on whether one or four electron bunches are stored in the synchrotron ring. Therefore we employed a high-speed mechanical chopper to reduce the rate to 1 KHz and a millisecond shutter to select single X-ray pulses on demand [5]. Synchronization between the laser and X-ray pulses was accomplished with ps precision using a Synchro-Lock-equipped Ti:sapphire laser (Coherent Mira). The low energy oscillator pulses were boosted to ~ 1 mJ in a regenerative amplifier (Spectra Physics Hurricane) and used to pump an OPA (Quantronix Topas), whose tunable output was stretched to the ps regime in a 3-m fiber prior to delivery to the protein crystal. X-ray pulses of $\sim 10^{10}$ photons/shot are generated when relativistic (6 GeV) electron bunches pass through the magnetic field of a 2-m long undulator. The mildly divergent X-ray radiation is focused by a toroidal mirror down to ~ 100 μm at a distance approximately 60 m from the source. The crystalline sample is positioned so that the X-rays pass through its upper edge, where the level of photolysis is greatest. The diffracted X-ray photons are detected with high quantum efficiency on a MAR CCD X-ray detector. Reconstruction of the protein structure with atomic resolution requires diffraction images from different crystal orientations spanning 60 degrees (owing to the six-fold symmetry of the crystal). With undulator radiation, the X-ray bandwidth is sufficient to obtain approximately 5-fold redundant data with images collected every 2 degrees. To obtain high dynamic range diffraction images with the available X-ray flux, approximately 8-32 X-ray shots were integrated on the MAR CCD before image readout. Because the protein crystal requires sufficient time to recover between photolysis pulses, which are intense enough to excite a significant fraction of the protein molecules, the maximum repetition rate used was 3.3 Hz. Diffraction images were accumulated with and without photolysis to generate accurate differences between the two diffraction data sets.

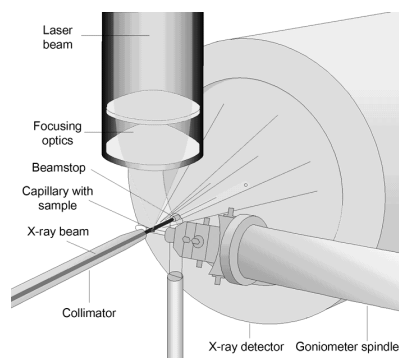


Fig. 1. Schematic diagram of the pump-probe geometry used to acquire time-resolved X-ray diffraction images.

3. Results and Discussion

The electron density of the protein is constructed by Fourier transforming appropriately scaled diffraction spot intensities (structure factors). The electron density for the unphotolyzed crystal is shown in Figure 2a. Because the photolysis is incomplete, the electron density of the photolyzed crystal, shown in Figure 2b, is a mixture of photolyzed and unphotolyzed states. To generate the electron density map for the photolyzed state, shown in Figure 2c, the fraction of photolysis was estimated, and the partially photolyzed electron density map was extrapolated to complete photolysis.

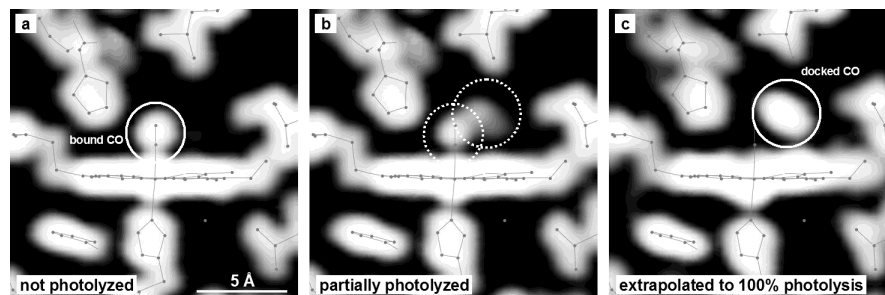


Fig. 2. (a) Electron density map of MbCO before photolysis. (b) Electron density of MbCO after about 25% photolysis (at 100 ps). Note the partial occupancy of CO in both binding and primary docking sites. (c) Electron density of the photolyzed state obtained after extrapolating the data from the middle image to complete photolysis.

High-resolution time-resolved electron density maps of wild-type and L29F MbCO are shown in Figures 3 and 4, respectively. These images were rendered using a novel color-coded method for visualizing structural changes. The images reveal, with atomic resolution, the order of events that accompany ligand translocation. Numerous features are observed in both wild-type and L29F MbCO, including the displacement of the heme iron toward the proximal histidine, tilting of the heme, docking of CO in a site near the heme iron, and the correlated motion of several protein side chains. However, dramatic differences are observed on the distal side of the heme, in particular the motion of the residues in the 29 and 64 positions. In wild-type MbCO, Leu29 moves upward and His64 shifts toward the site once occupied by CO, raising the barrier to geminate recombination. In L29F MbCO, Phe29 is pushed toward H64, which shifts down and away from the heme iron, and displaces a water molecule on the surface of the protein. Only when the CO departs from the primary docking site does the His64 side chain assume a position similar to that found with wild-type Mb. On the nanosecond time scale, CO slips around to the other side of the heme and is found in the so-called Xe1 docking site. The CO escapes from this site into the surrounding solvent on the microsecond time scale. On the millisecond time scale, CO rebinds with the heme and completes the photocycle. The cycle can be repeated thousands of times without appreciable damage to the protein crystal.

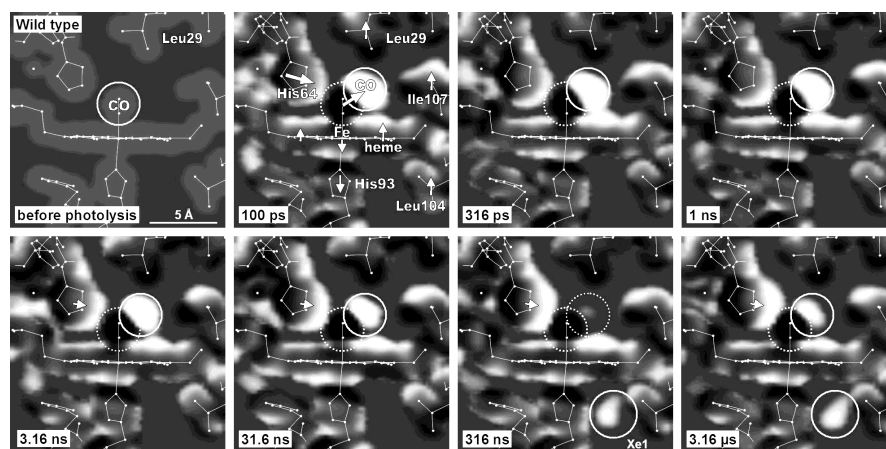


Fig. 3. Electron density maps of wild-type MbCO determined before and at various times after photolysis at 10 °C. The electron density of the unphotolyzed protein is colored black while that of the photolyzed protein is colored white. Where both densities overlap, the two shades blend to gray. The direction of molecular motion follows the black to white gradient. The white stick models correspond to the static crystal structures, and are included to guide the eye. The solid circles denote occupied CO sites and the dotted circles denote evacuated CO sites. The photolyzed CO is initially trapped in the primary docking site about 2 Å from the binding site, but subsequently migrates to the Xe1 site on the opposite side of the heme.

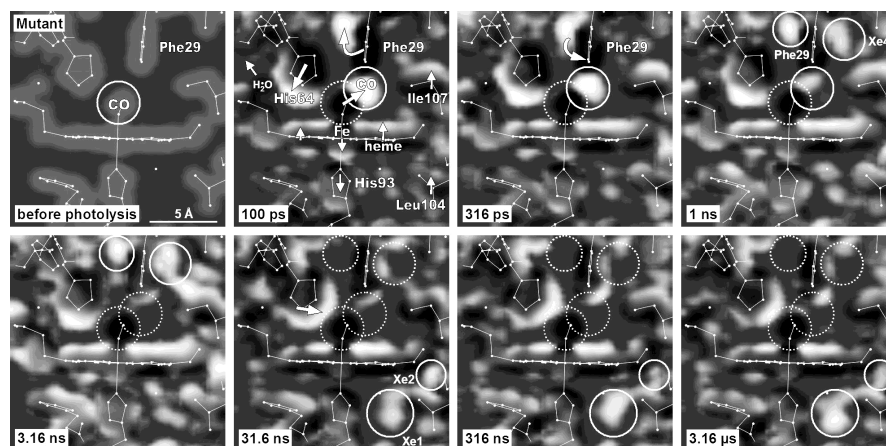


Fig. 4. Electron density maps of L29F MbCO determined before and at various times after photolysis at 10 °C. Soon after photolysis, CO migrates to sites labeled Phe29 and Xe4. The CO continues its migration with a significant fraction of the CO accumulating in Xe1 and possibly Xe2. The most dramatic differences in the side chain motion of wild-type and L29F Mb are manifested in the sub-ns maps, demonstrating the need to probe protein dynamics on a sub-ns time scale.

4. Conclusions

The mechanism for excreting toxic CO in the wild-type and mutant MbCO is different. In wild-type protein, His64 rapidly relaxes toward the heme iron, which protects it from CO rebinding. In L29F MbCO, the strain induced on Phe29 and His64 by docked CO is rapidly relieved when Phe29 “sweeps” the CO away from the primary docking site. Though the mechanism of excretion is different, both are effective. The structural changes that accompany ligand translocation, as illustrated here, help explain how the protein is able to excrete toxic CO with high efficiency, even though the CO is temporarily located so close to the active binding site. Clearly, time-resolved crystallographic studies can unveil at a high level of structural detail the conformational changes that accompany protein function in this and other protein systems. The fact that global conformational changes are apparent at 100 ps, the earliest time point recorded, demonstrates that much higher time resolution will be required to follow the protein quake that ensues after ligand photolysis. This phase of the conformational motion will be accessible to 4th generation X-ray sources, which promise to deliver intense, sub 100-fs X-ray pulses [6,7].

Acknowledgements. We thank Prof. J.S. Olson and Dr. J. Soman for supplying the P6 MbCO crystals used in this study. We thank G. Hummer for helpful comments and D. Bourgeois for sharing his expertise in the analysis of Laue diffraction data.

References

- 1 V. Srajer et al., *Science* **274**, 1726-9., 1996.
- 2 Q. H. Gibson, S. Ainsworth, *Nature* **180**, 1416-7, 1957.
- 3 T. E. Carver et al., *J. Biol. Chem.* **267**, 14443-14450, 1992.
- 4 F. Schotte et al., *Science* **300**, 1944-7, 2003.
- 5 F. Schotte et al., in *Third-Generation Hard X-ray Synchrotron Sources* D. M. Mills, Edited by D. M. Mills, Wiley and Sons, New York, 2002
- 6 A. Cho, *Science* **296**, 1008-10., 2002.
- 7 M. Abd-Elmeguid et al., in *TESLA: The Superconducting Electron-Positron Linear Collider with Integrated X-ray Laser Laboratory - Technical Design Report* G. Materlik, T. Tschentscher, Edited by G. Materlik, T. Tschentscher, DESY, Hamburg, 2001